In Vitro Cellular & Developmental Biology - Animal
https://doi.org/10.1007/s11626-024-00927-x

Spatiotemporal distribution of PTEN before directed cell migration in monolayers

Quanzhi Lu[1] · Saori Sasaki[2] · Toshihiro Sera[3] · Susumu Kudo[2]

Received: 22 February 2024 / Accepted: 12 May 2024 / Editor: Masakiyo Sakaguchi
© The Society for In Vitro Biology 2024

Abstract
The intracellular distribution of phosphatase and tensin homolog (PTEN) is closely related to directed cell migration. In single cells, PTEN accumulates at the rear of the cell before and during directed migration; however, the spatiotemporal distribution of PTEN in confluent cell monolayers, particularly before directed migration, remains unclear. In this study, we wounded a cell in confluent fetal rat skin keratinocytes (FRSKs) and examined the dynamics of PTEN in the cells adjacent to the wounded cell. In contrast to single-cell migration, we found that PTEN translocated to the nucleus before the beginning of directed migration. This nuclear translocation of PTEN did not occur in disconnected cells, and it was also suppressed by importin-β inhibitor and actin inhibitor. When the nuclear localization of PTEN was inhibited by an importin-β inhibitor, cell elongation in the direction of migration was also significantly inhibited. Our results indicate that PTEN translocation is induced by the disruption of cell–cell adhesion and requires the involvement of importin-β and actin cytoskeleton signaling. In addition, phosphatidylinositol 3,4,5-triphosphate (PIP3) may regulate PTEN distribution through its localized accumulation at the cell edge. Our findings suggest that the translocation of PTEN is crucial for directed cell migration and for responding to mechanical environmental changes in confluent cell monolayers.

Keywords Phosphatase and tensin homolog · Phosphatidylinositol 3,4,5-triphosphate · Wound · Translocation · Cell migration

Introduction

Phosphatase and tensin homolog (PTEN) is a dual-specificity lipid and protein phosphatase. Mutations in PTEN are associated with various cancers (Steck *et al.* 1997). PTEN regulates the dephosphorylation of phosphatidylinositol 3,4,5-triphosphate (PIP3) to form phosphatidylinositol 4,5-bisphosphate (PIP2) (Campbell *et al.* 2003). Thus, PTEN can suppress the phosphoinositide 3-kinase (PI3K) pathway and inhibit downstream signaling events that regulate cell migration (Stambolic *et al.* 1998; Tamura *et al.* 1998). In addition, PTEN plays an important role in modulating actin dynamics (Li *et al.* 2014), which is important for cell movement and mediating the direction of cell migration (Fife *et al.* 2014).

Chemotaxis is the process by which cells migrate directionally along gradients of chemoattractants, such as adenosine 3′,5′- cyclic monophosphate (cAMP) (Xu *et al.* 2005). The cytoplasmic distribution of PTEN is essential for the directed migration of single cells (Funamoto *et al.* 2002). In experiments with Dictyostelium, individual cells moved rapidly toward a micropipette approximately 40 s after the addition of 1 μmol L^{-1} cAMP (Parent *et al.* 1998). Before this directed migration began, PTEN decreased at the front edge of the cell and accumulated at the rear of the cell 15 s after the cells were exposed to a chemoattractant gradient and PTEN was continuously distributed at the rear of the cell during directed migration (Funamoto *et al.* 2002). In contrast, PIP3, a substrate of PTEN, was localized at the

✉ Susumu Kudo
kudo.susumu.237@m.kyushu-u.ac.jp

1 Department of Mechanical Engineering, Graduate School of Engineering, Kyushu University, 744 Motooka, Nishi-Ku, Fukuoka-Shi, Fukuoka 819-0395, Japan

2 Department of Mechanical Engineering, Faculty of Engineering, Kyushu University, 744 Motooka, Nishi-Ku, Fukuoka-Shi, Fukuoka 819-0395, Japan

3 Department of Medical and Robotic Engineering Design, Faculty of Advanced Engineering, Tokyo University of Science, 6-3-1 Niijuku, Katsushika-ku, Tokyo 125-8585, Japan

Published online: 26 June 2024

front edge of neutrophil-differentiated HL-60 cells 13 s after the addition of the chemoattractant before the directional migration began and continued to accumulate at the front edge of the cells (Servant *et al.* 2000). This may be related to localized actin polymerization and pseudopodia formation. In addition, loss of PTEN promoted cytoskeletal rearrangement (Lin *et al.* 2015). PTEN-deficient Dictyostelium cells did not migrate toward the micropipette following cAMP exposure and filamentous actin levels were sixfold higher compared with that of wild-type cells 120 s after the addition of 1 μmol L^{-1} cAMP; this suggests that defective chemotaxis is specifically the result of the loss of PTEN (Iijima and Devreotes 2002). The local distribution of PTEN and PIP3 yields cells with functionally and morphologically distinct front and rear edges (Arai *et al.* 2010). PTEN is involved in directional sensing and PTEN is localized at an early stage before directed migration in single cells.

In confluent cell monolayers, directed migration can be induced by mechanical scratching or wounding. Surrounding cells initiate migration to the wounded area when the monolayer is scratched with a micropipette tip. In particular, when confluent MCF7 cells are mechanically wounded, surrounding cells migrate to the site of the wound within 24 h and a loss of PTEN can enhance this directed migration (Heering *et al.* 2009). Besides, a loss of PTEN enhanced the velocity and distance of migration in a monolayer of astrocyte cells 24 h after scratching by a microinjection needle, which was correlated with PTEN controlling cell–cell junctions to influence intracellular actin in moving cells (Peglion *et al.* 2022). In addition, after the monolayer was scratched, human glioma cells migrated to the wound area within 16 h. PTEN inhibits this directed migration by disturbing the process through its C2 domain (Raftopoulou *et al.* 2004). In lung epithelial monolayers, PTEN inhibition resulted in a decrease in cell stiffness near the wound edge, which in turn significantly enhanced the directed migration 2 h after scratching (Mihai *et al.* 2012). Although the inhibitory effect of PTEN has been well-studied, there are no reports describing the intracellular localization of PTEN in monolayers, particularly before directed migration.

The localization of PTEN in the cell nucleus has been found to be related to cell proliferation, apoptosis, and cellular stability (Planchon *et al.* 2008). The PTP and the C2 domains of PTEN contain several nuclear localization signal (NLS)–like sequences (Chung *et al.* 2005; Chung and Eng 2005), which are important for controlling PTEN's subcellular localization and function (Gil *et al.* 2007). Mutations in the PTEN N-terminal region affect its nuclear localization and the ability of PTEN to regulate mammalian cell growth (Denning *et al.* 2007; Gil *et al.* 2015). The presence of PTEN in the nucleus is regulated by complex mechanisms, including diffusion (Liu *et al.* 2005), monoubiquitylation-dependent import (Baker 2007), and interactions with major vault protein (MVP) (Chung *et al.* 2005). Furthermore, the binding and dissociation of the small GTPase Ran to importin-β proteins are necessary for importin-mediated nuclear transport (Görlich and Kutay 1999). Coexpression of a dominant negative Ran GTPase protein has been shown to inhibit PTEN accumulation in the nucleus, suggesting that importin-β may play an active role in PTEN nuclear accumulation (Gil *et al.* 2006). Therefore, clarifying the relationship between importin proteins and PTEN nuclear localization is crucial for a more comprehensive insight into PTEN's subcellular localization mechanisms. Specifically, we investigated the influence of importin-β inhibition on PTEN nuclear localization before directed cell migration.

Single-cell migration is based on the formation and rearrangement of front-rear polarity orientation, which is related to the intracellular distribution of PIP3 and PTEN (Gerisch *et al.* 2012). In particular, the spatiotemporal distribution of PTEN and PIP3 has been studied in single cells. The response of PTEN occurs at an early stage before directed migration begins, highlighting their important roles in determining cell directionality. However, in confluent cell monolayers, unlike single cells, each cell is surrounded by neighboring cells, in which stable interconnections and mutual constraints are present (Scarpa and Mayor 2016). Thus, cell migration in monolayers exhibits different mechanisms compared with that of single cells. However, there is little information regarding the status of PTEN specifically before directed migration, although there have been studies describing the role of PTEN during directed migration. Therefore, understanding its state before migration is essential for initiating cell migration in monolayers. In this study, we wounded one cell in confluent fetal rat skin keratinocytes (FRSKs) and examined the spatiotemporal distribution of PTEN in the cells adjacent to the wound before the start of directed migration. In addition, we determined the effects of the actin cytoskeleton and importin-β on the dynamics of PTEN.

Materials and methods

Cell culture Fetal rat skin keratinocytes (FRSKs) were purchased from the Japanese Cancer Research Bank (Japan) in September 2023 and were serially passaged, proliferating for less than 6 mo. FRSKs were cultured using Dulbecco's modified Eagle's medium (DMEM; Gibco™, Thermo Fisher Scientific, Waltham, MA) containing 10% fetal bovine serum (Biological Industries, Kibbutz Bei t-Haemek, Israel) and a 1% antibiotic–antimycotic solution (10,000 U ml^{-1} penicillin, 10,000 μg ml^{-1} streptomycin, and 25 μg ml^{-1} amphotericin B, Gibco™, Thermo Fisher Scientific, Waltham) in a humidified incubator containing 5% CO_2 at 37 °C.

cDNA and transfection GFP-PTEN was a gift from Alonzo Ross (Addgene plasmid #13,039; http://n2t.net/addgene:13039; RRID:Addgene_13039). PH-Akt-GFP was a gift from Tamas Balla (Addgene plasmid #51,465; http://n2t.net/addgene:51465; RRID:Addgene_51465). pcDNA3-mRFP was a gift from Doug Golenbock (Addgene plasmid #13,032; http://n2t.net/addgene:13032; RRID:Addgene_13032). pcDNA3-EGFP-Rac1(wt) was a gift from Klaus Hahn (Addgene plasmid #13,719; http://n2t.net/addgene:13719; RRID:Addgene_13719).

FRSKs were seeded into a 35 mm glass-bottomed dish and cultured to 60–70% confluence prior to transfection. The cells were washed twice with Opti-MEM (Gibco™; Thermo Fisher Scientific) and cultured for 1 h with 1 ml Opti-MEM as the medium. Then, 2 µl of 1 µg μl^{-1} DNA (GFP-PTEN, PH-Akt-GFP, pcDNA3-EGFP-Rac1, or pcDNA3-mRFP) and 4 µl of HilyMax (Dojindo Laboratories, Kumamoto, Japan) were mixed in 100 µl of Opti-MEM and the mixture was added to the glass dish. After a 4-h incubation, the medium was replaced with 2 ml of DMEM (10% fetal bovine serum, no antibiotics) at 37 °C. The FRSKs grown to confluence were used for experiments 24 h following transfection.

Calcium imaging Fura-2-acetoxymethyl ester (Fura-2-AM; Invitrogen, Carlsbad, CA) was used as a Ca^{2+} indicator. Transfected FRSKs in each dish were washed twice with 1 ml 4-(2-hydroxyethyl)-1-piperazineethanesulfonic acid (HEPES)–buffered saline (HBS) and loaded with 5 µmol L^{-1} Fura-2-AM in HBS for 30 min at 25 °C. Transfected FRSKs in each dish were washed twice with 1 ml HBS and 2 ml of HBS was added as the buffer for observation. Images of Fura2-AM were observed following excitation at 380 nm and fluorescence at 510 nm.

Treatment with inhibitors N-(1-Phenylethyl)-2-(pyrrolidin-1-yl)quinazolin-4-amine (Importazole; Focus Biomolecules, Plymouth Meeting, PA) is a specific inhibitor for importin-β-mediated nuclear import in cells. A 20 mmol L^{-1} Importazole solution was diluted to 40 µmol L^{-1} before treatment. Transfected FRSKs in some dishes were washed twice with 1 ml HBS and a 40 µmol L^{-1} Importazole solution was added. Then, the FRSKs were prepared for experiments after a 30-min incubation.

(3S,3aR,4S,6S,6aR,7E,10S,12R,13E,15R,15aR)-15-(acetyloxy)-3,3a,4,5,6,6a,9,10,12,15-decahydro-6,12-dihydroxy-4,10,12-trimethyl-5-methylene-3-(phenylmethyl)-1H-cycloundec[d]isoindole-1,11(2H)-dione (cytochalasin D; FUJIFILM Wako Pure Chemical Corporation, Osaka, Japan) was used as an inhibitor of the actin cytoskeleton. A 1.0 mmol L^{-1} cytochalasin D solution was diluted to 2.5 µmol L^{-1} before treatment. Transfected FRSKs in some dishes were washed twice with 1 ml HBS and 2.5 µmol L^{-1} cytochalasin D solution was added. Then, the FRSKs were prepared for experiments after a 30-min incubation.

Mechanical wounding and imaging In confluent cell monolayers, cells tend to migrate toward the wounded area after a wound is generated with a fine glass micropipette (Arai *et al.* 2017). A micropipette puller (P-97; Sutter Instrument Company, Novato, CA) was used to melt and stretch a borosilicate tube for making the fine glass micropipette, which was less than 3 µm in diameter. A single cell was mechanically wounded using a fine glass micropipette in a monolayer FRSKs. A manipulator (InjectMan 4; Eppendorf, Germany) was used to control the micropipette approach to the cell. When the micropipette tip approached the target cell, the cell was stimulated by immediately dropping the micropipette. We determined whether the cell was wounded successfully by observing a decrease in the fluorescent intensity of the Ca^{2+} indicator Fura2-AM (Supplement Movie 1). The results of fluorescence recovery were considered an unsuccessful wound and were excluded from the statistical analysis. On each experimental day, we prepared 3 culture dishes and measured 2–3 cells for each dish during the experiment. N represents the total number of culture dishes and n represents the total number of cells. An inverted microscope (Eclipse TE2000-S; Nikon Corp., Tokyo, Japan) fitted with a 40 × oil-immersion lens (S-Fluor, numerical aperture = 1.3; Nikon Corp.) was used to observe the expression of GFP-PTEN, PH-Akt-GFP, and the change in protein distribution within the cell. The excitation wavelength was cycled between 380, 488, and 583 nm to observe the fluorescence of intracellular Ca^{2+}, Green Fluorescent Protein (GFP), and Monomer Red Fluorescent Protein (mRFP). ImageJ software was used to process and analyze the fluorescent images (Schneider *et al.* 2012). The images of GFP and mRFP were visually displayed in green and red, respectively. Because fluorescence gradually decreases with time, all of the figures in this study were subject to fading correction by dividing the fade ratio (Supplement Fig. 1) at the corresponding time using "Process-Math" in ImageJ. The fluorescence intensity at any time divided by the initial fluorescence intensity at 0 min was used to define the relative intensity, which represents the level of the observed subjects in the regions of interest (ROI). Images of translocation are obtained by adding a value of 128 to the original image and then subtracting the original image captured at $t = 0$ min using the "Process-Image Calculator" in ImageJ. The initial cell outline is utilized as a reference for images depicting translocation, preventing the impact of local cellular deformations on the resultant image. Furthermore, the initial background value of the resulting image is set to 0.

Quantitative analysis of cell elongation for determining the initiation of cell migration Rac1 localizes anterior to the front edge of migrating cells (Yamao *et al.* 2015).

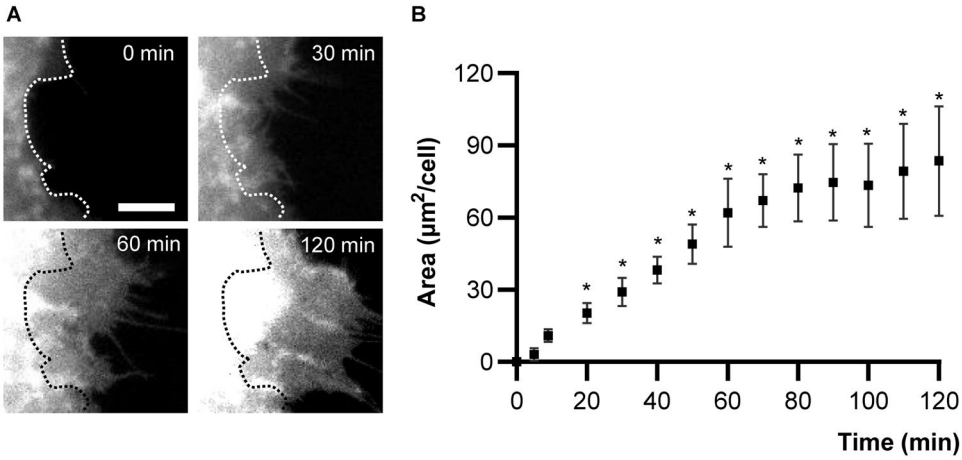

Figure 1. Cell elongation at the edge after neighbor cell wounding. (***A***) Images of the cell including EGFP-Rac1 after neighboring cell wounding. Cell boundaries at 0 min are indicated by the *dotted line*. *White scale bar*: 5 μm. (***B***) Quantification of the cell elongation area in a time series after wounding. $N=9$, $n=16$. Mean ± standard error of the mean. $^{*}P<0.05$ vs. 1 min (two-way ANOVA with post hoc Dunnett's test).

Therefore, we analyzed the area including EGFP-Rac1 as the area of cell elongation after wounding. The elongation of FRSKs was calculated from the resulting images. Because cell migration begins with anterior signaling and protrusion formation (Ridley *et al.* 2003), we analyzed the area protruding after 1 min as the cell elongation after wounding. When cells significantly elongate, it is considered that cell migration has begun.

Statistical analysis Statistical analyses included an analysis of variance. Multiple comparisons were performed using a two-way ANOVA followed by Dunnett's test or Sidak's test. A P value <0.05 was considered a statistically significant difference, whereas ns indicates not significant. All graphs are presented as the mean ± standard error of the mean. The number of glass dishes and cells are denoted by N and n, respectively.

Results

Cells start to migrate 10 min after neighboring cells are wounded To determine the time before initiation of the directed migration in confluent cell monolayers, we examined the area of cell elongation. Figure 1*A* shows images of FRSKs, including EGFP-Rac1, after wounding its neighboring cells in monolayers. The FRSKs were gradually elongated over time toward the wounded area. Figure 1*B* shows that the average elongation area per cell increased over time after wounding. There was no statistically significant difference within the first 10 min following wounding; however, the elongation area after 20 min was statistically larger compared with that after 1 min. Because elongation at the edges of the cells is considered an early event in directed cell migration, we defined the time between 0 and 10 min after wounding as the period before cell migration. During this period, we examined the spatiotemporal distribution of PTEN and its substrate PIP3.

PTEN translocated to the nucleus before directed migration Figure 2 shows the dynamics of GFP-PTEN before directed migration in FRSKs. Figure 2*A* and *B* show the fluorescent images of the GFP-PTEN translocation within the cells. The fluorescence of GFP-PTEN decreased in the area near the wounded cell and increased in the nucleus (Supplement Movie 2 and 3). To eliminate the potential influence of fluorescent protein on PTEN nuclear localization, we also observed the Monomer Red Fluorescent Protein (mRFP) before directed migration by co-transfecting pcDNA3-mRFP and GFP-PTEN. In contrast to GFP-PTEN, the mRFP did not exhibit any sustained changes in the cell nucleus (Fig. 2*C*). Considering the cytoplasmic and nuclear localization of PTEN, we designated three regions of interest (ROIs) as near, far, and nucleus in the cells based on the distance from the wounded cell (Fig. 2*D*); the near and far ROI were within a maximum distance of 4 μm away from the edge of the cell (Arai *et al.* 2017). Figure 2*E* shows the changes in the relative fluorescent intensity of GFP-PTEN. The relative fluorescence intensity was significantly lower after 40 s in the near ROI than that at 0 min, and reached a minimum value of 0.85 ± 0.03 at 2 min. In contrast, the relative fluorescence intensity in the nucleus ROI increased and reached a maximum value of 1.11 ± 0.01 at 10 min. The relative fluorescence intensity after 2 min was significantly higher than that at 0 min in the nucleus. Furthermore, we examined the relative fluorescent intensity of mRFP in the nucleus. The relative fluorescent intensity of mRFP remained close to the initial value of 1.0 after 5 min and was

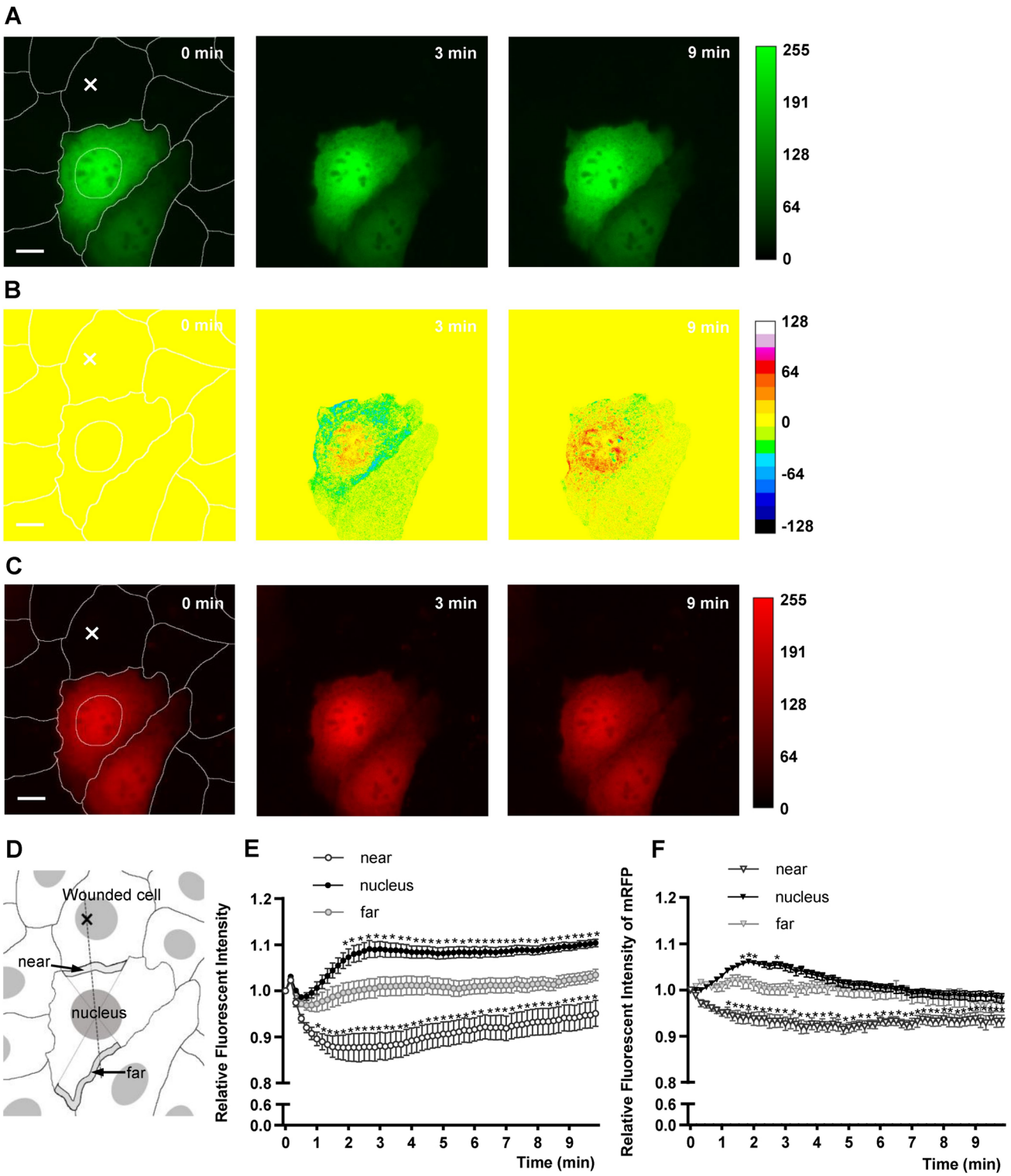

Figure 2. The dynamics of GFP-PTEN before directed migration in monolayers. (***A***) Representative fluorescence images of GFP-PTEN before directed migration. (***B***) Images of GFP-PTEN translocation obtained by subtracting the original image in (***A***) captured at $t=0$ min and setting the initial value as 0. The intensity of GFP-PTEN is shown using a pseudo color scale. Greater than 0 is considered an increase compared with the initial value. (***C***) The fluorescence images of pcDNA3-mRFP before directed migration. Cell boundaries and nucleus boundaries at 0 min are indicated by *white line*. "×" indicates the wounded cell. *White scale bar*: 10 μm. (***D***) The region of near, far, and nucleus in the cells. (***E***) Relative fluorescent intensity of GFP-PTEN in a time series. (***F***) Relative fluorescence intensity of pcDNA3-mRFP in a time series. $N=8$, $n=16$. Mean ± standard error of the mean. $^{*}P<0.05$ vs. 0 min (two-way ANOVA with post hoc Dunnett's test).

not significantly different from that at 0 min (Fig. 2*F*). These results suggest that PTEN translocates from the cytoplasm to the nucleus after neighboring cell wounding and before directed migration in monolayers.

Effects of Importazole on PTEN nuclear translocation and directed cell migration after neighboring cell wounding The nuclear translocation of PTEN may require the involvement of transport proteins. To gain further insight into the PTEN response, we used Importazole as an inhibitor for importin-β-mediated nuclear import and examined the dynamics of PTEN after neighboring cell wounding during Importazole treatment (Fig. 3*A, B*). We examined the relative fluorescence intensity, and GFP-PTEN showed no difference in relative fluorescence intensity compared to 0 min in the nucleus (Fig. 3*C*). Moreover, there was a significant difference in the relative fluorescence intensity of GFP-PTEN after 4 min between the Importazole-treated and untreated groups (Fig. 3*D*). Importazole treatment inhibited the PTEN response, indicating that importin-β may be involved in the nuclear translocation of PTEN after wounding in confluent cell monolayers. The effect of Importazole treatment on directed cell migration was also examined. Figure 4*A* is an image of FRSK after neighboring cell wounding with Importazole treatment. Figure 4*B* shows that the average elongation area per cell increased with time after neighboring cell wounding; the elongation area at 30 min was significantly smaller than that of the untreated control. Importazole treatment inhibited the increase in cell elongation, suggesting an active role in the nuclear localization of PTEN in directed cell migration in cell monolayers.

Accumulation of PIP3 before directed migration The PIP3 signal may play a potential role in PTEN localization; we examined PIP3 dynamics using the indicator PH-Akt-GFP before directed migration (Fig. 5). Figure 5*A* and *B* show the fluorescent images of the PH-Akt-GFP translocation in the cells. The fluorescence of PH-Akt-GFP increased in the region near the wounded cell (Supplement Movie 4 and 5). We examined the relative fluorescence intensity in the near, far, and nucleus ROI in the cells based on the distance from the wounded cell (Fig. 5*C*). The relative fluorescence intensity of PH-Akt-GFP was increased in the near ROI and reached a maximum value of 1.36 ± 0.03 at 10 min (Fig. 5*D*). The relative fluorescence intensity after 2 min in the near ROI was significantly higher than that at 0 min. In contrast, the relative fluorescent intensity in the nucleus ROI and far ROI showed no significant change compared to that at 0 min. Both the increase in PH-Akt-GFP and the decrease in GFP-PTEN occurred in the near ROI, suggesting that the translocation of PTEN may contribute to the directional accumulation of PIP3 before directed migration in monolayers. To investigate the effect of PTEN nuclear localization on PIP3 accumulation, we examined the intracellular translocation of PH-Akt-GFP after neighbor cell wounding with addition of Importazole (Fig. 6). Figure 6*A* and *B* show PH-Akt-GFP fluorescence images of Importazole-treated cells, with a slight accumulation at the cell edge near the wounded cells; the relative fluorescence intensity of PH-Akt-GFP increased in the near ROI and reached a maximum value of 1.13 ± 0.02 at 10 min (Fig. 6*C*). Although there was an increase in relative fluorescence intensity in the near ROI, the Importazole treatment group showed significantly lower intensity than the untreated group (Fig. 6*D*). These results indicate that inhibition of PTEN nuclear translocation inhibits PIP3 accumulation, suggesting that the nuclear localization of PTEN may play a role in regulating PIP3 accumulation in cell monolayers.

PTEN and PIP3 do not translocate after wounding when cells are separated Neighbor cell wounding is accompanied by leakage of cellular content and the disruption of cell–cell adhesion. To determine what induces the response of PTEN and PIP3, we wounded cells near, but without direct cell–cell adhesion, to the target cell. Figure 7 shows the dynamics of PTEN and PIP3 after wounding when the cells were separated. Figure 7*B* and *D* represent the fluorescent images using the GFP-PTEN and PH-Akt-GFP constructs, respectively. PTEN did not translocate to the nucleus and PIP3 did not accumulate at the cell edge near the wounded cells. Using the same definition of ROIs as in Fig. 2*D*, the relative fluorescence intensity of GFP-PTEN (Fig. 7*E*) or PH-Akt-GFP (Fig. 7*F*) was not significantly different in any of the ROIs within 10 min. Even if nearby cells were wounded, there was no translocation of PTEN or PIP3 in the absence of intercellular adhesion. This suggests that it is not the leakage of cell contents, but the disruption of cell–cell adhesion that induces the localized distribution of PTEN and PIP3.

Actin cytoskeletal affects PTEN translocation The actin cytoskeleton plays an important role in cell–cell adhesion and is responsible for generating the force that holds cells together (Vasioukhin *et al.* 2000). Cytochalasin D destabilizes and displaces actin filaments, causing them to detach from their normal attachment points, which results in the disruption of the actin cytoskeleton (Wakatsuki 2001). To determine the effect of the actin cytoskeleton on PTEN dynamics, we used cytochalasin D as an actin inhibitor and examined PTEN localization after neighbor cell wounding in monolayers. Figure 8*A* and *B* show the fluorescence images of cytochalasin D–treated cells. Using the same definition for the ROIs as Fig. 2*D*, we examined the relative fluorescence intensity in the near, far, and nucleus ROI (Fig. 8*C*). Except for a very slight decrease in the near ROI at 1–2 min after wounding, the relative fluorescence intensity of

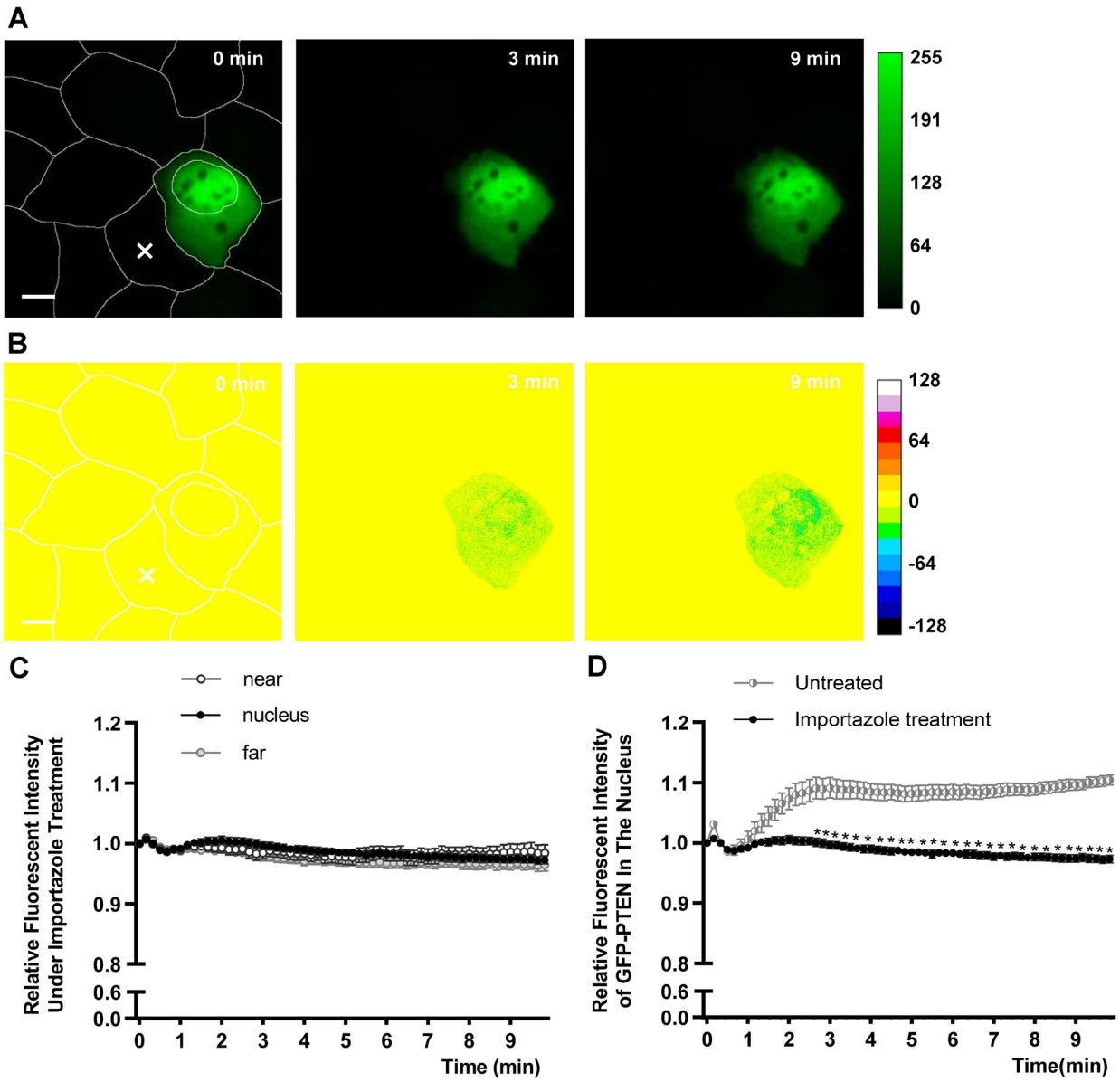

Figure 3. The effect of the importin-β inhibitor Importazole. (***A***) Representative fluorescence images of GFP-PTEN during treatment with Importazole (40 μmol L^{-1}) before directed migration. (***B***) Images of GFP-PTEN translocation obtained by subtracting the original image in (***A***) captured at $t=0$ min and setting the initial value as 0. The intensity of GFP-PTEN is shown using a pseudo color scale. Greater than 0 is considered an increase compared with the initial value. Cell boundaries and nucleus boundaries at 0 min are indicated by *white line*. "×" indicates the wounded cell. *White scale bar*: 10 μm. (***C***) Relative fluorescent intensity of GFP-PTEN under Importazole treatment. $N=8$, $n=16$. Mean ± standard error of the mean. $^{*}P<0.05$ vs. 0 min (two-way ANOVA with post hoc Dunnett's test). (***D***) Comparison of GFP-PTEN relative fluorescence intensity in the nucleus with Fig. 2*E*. $N=8$, $n=16$. Mean ± standard error of the mean. $^{*}P<0.05$ vs. untreated (two-way ANOVA with post hoc Sidak's test).

GFP-PTEN showed no significant difference in all ROIs compared with that at 0 min. The relative fluorescent intensity of GFP-PTEN was compared with the untreated group for the nucleus ROI (Fig. 8*D*). There was a significant difference after 5 min between the cytochalasin D–treated group and the untreated group. These results suggest that the inhibition of actin suppresses the nuclear translocation of PTEN in monolayers.

Discussion

As opposed to directed migration in single cells, this study represents the first report demonstrating that PTEN translocates to the nucleus before directed migration begins in cell monolayers, without accumulating at the rear of the cell. In contrast, PIP3, a substrate for PTEN, accumulates in the periphery closest to the wounded cells.

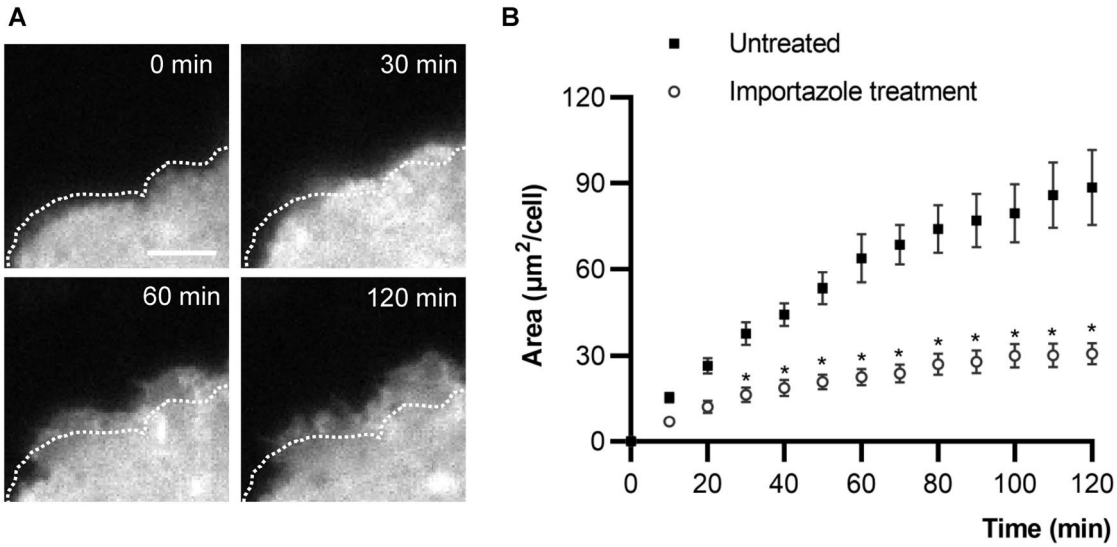

Figure 4. Cell elongation at the edge after neighbor cell wounding under Importazole treatment. (***A***) Images of the cell including EGFP-Rac1 after neighbor cell wounding with Importazole treatment (40 μmol L^{-1}). Cell boundaries at 0 min are indicated by the *dotted line*. *White scale bar*: 5 μm. (***B***) Quantification of the cell elongation area in a time series after wounding. $N=8$, $n=11$. Mean ± standard error of the mean. $^{*}P<0.05$ vs. untreated (two-way ANOVA with post hoc Sidak's test).

Furthermore, we found that Importazole treatment inhibits PTEN nuclear translocation and directs cell migration following neighbor cell wounding. Moreover, cell–cell adhesion is essential for the translocation of PTEN and PIP3; specifically, PTEN and PIP3 exhibited no response after wounding when the cells were separated.

Directed migration in single cells correlates with actin polymerization and disassembly on the sides of the cell (Stock and Pauli 2021). There are no cell–cell adhesions in single cells and the response of PTEN occurs at an early stage before directed migration begins. However, cells in a monolayer are closely packed and cell–cell adhesion links adjacent cells together, which provides mechanical support and facilitates communication (Mayor and Etienne-Manneville 2016). Cell–cell adhesion is a significant factor that influences directed migration (Saraswathibhatla *et al.* 2020). Therefore, we believe that the different phenomenon observed for PTEN in the present study compared with single cells is the result of cell–cell adhesion.

In monolayers, PTEN translocates to the nucleus after neighbor cell wounding (Fig. 2) and this nuclear translocation is suppressed by an actin inhibitor (Fig. 8). We previously reported that wounding of neighboring cells leads directly to the unloading of intercellular stress and the disruption of intercellular adhesion results in a larger strain field of the substrate in areas adjacent to wounded cells (Sera *et al.* 2019). In addition, mechanical forces generated by the dynamic rearrangements of cell–cell adhesion and the cytoskeleton cause changes in cell shape and motility (Jamora and Fuchs 2002). In the present study, neighbor cell wounding was accompanied by the disruption of cell–cell adhesion. When the actin cytoskeleton was inhibited with cytochalasin D, cell–cell adhesion and the mechanical properties of the cells were negatively affected and the nuclear translocation of PTEN was significantly inhibited. In contrast, there was no translocation of PTEN when the cells were subconfluent (Fig. 7), suggesting a dependence upon mechanical force sensing for cell–cell adhesion. These results indicate the nuclear translocation of PTEN requires mechanical stimulation and the intact actin cytoskeleton, which regulates the spatial distribution of PTEN.

Unlike its distribution in single cells, PTEN does not accumulate at the rear of the cell before directed migration begins in monolayers (Fig. 2*A, B*). PTEN can negatively regulate cell interactions with the extracellular matrix (ECM) by decreasing the formation of actin filaments and focal adhesions (Tamura *et al.* 1998). In addition, cell-ECM adhesion or cytoskeletal contractility can affect cell surface scaffolds, which regulates single-cell and collective-cell migration (Friedl and Alexander 2011). Impaired intercellular adhesion and loss of adherens junctions result in the detachment of cells (Young 2003). Therefore, cells may need to stably adhere to the ECM and surrounding cells in monolayers, unlike the situation in single-cell migration. PTEN does not accumulate at the rear of the cell to mediate rear contractility, guaranteeing high mechanical stability in monolayers.

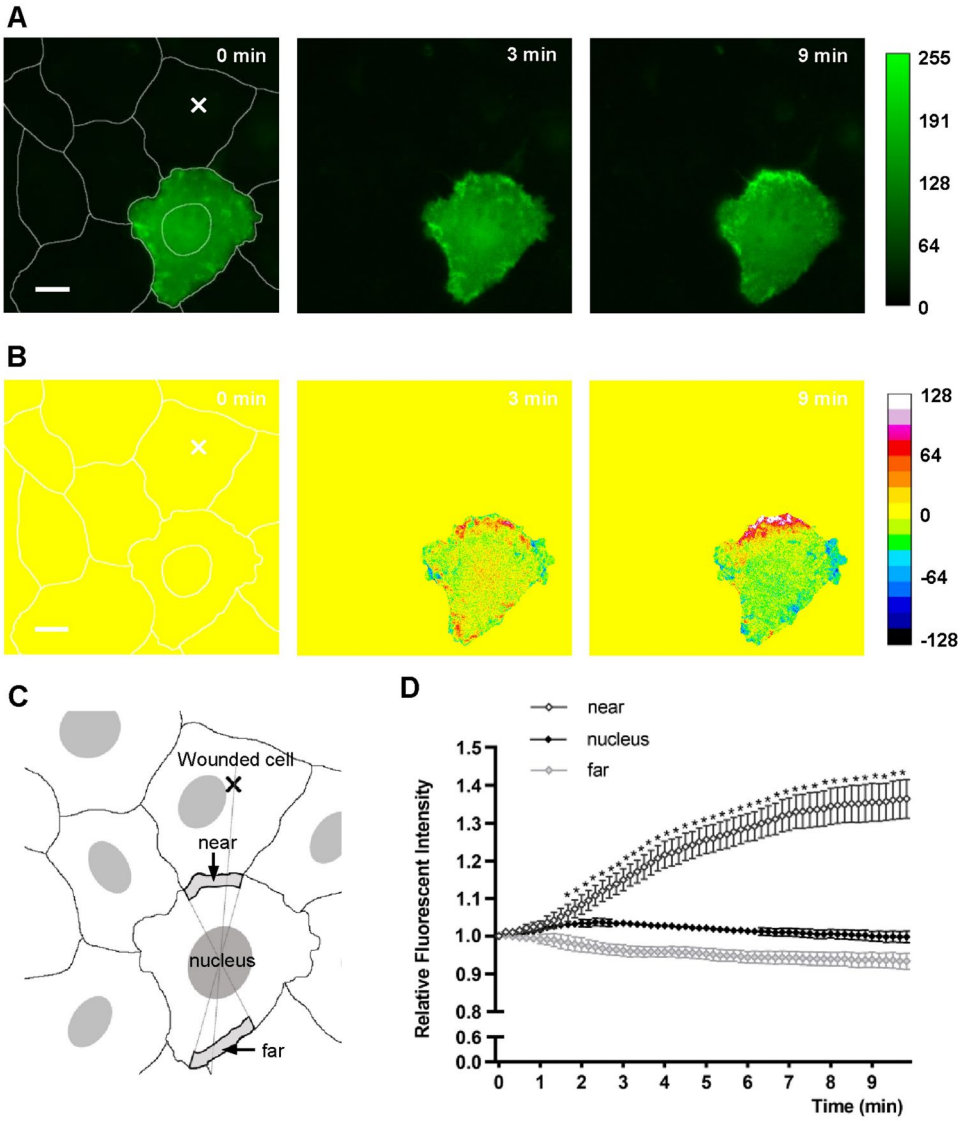

Figure 5. The dynamics of PH-Akt-GFP before directed migration in monolayers. (***A***) Representative fluorescence images of PH-Akt-GFP before directed migration. (***B***) Images of PH-Akt-GFP translocation obtained by subtracting the original image in (***A***) captured at $t = 0$ min and setting the initial value as 0. The intensity of PH-Akt-GFP is shown using a pseudo color scale. Greater than 0 are considered an increase compared with the initial value. Cell boundaries and nucleus boundaries at 0 min are indicated by *white line*. "×" indicates the wounded cell. *White scale bar*: 10 µm. (***C***) The region of near, far, and nucleus in the cells. (***D***) Relative fluorescent intensity of PH-Akt-GFP in a time series. $N = 14$, $n = 32$. Mean ± standard error of the mean. $^{*}P < 0.05$ vs. 0 min (two-way ANOVA with post hoc Dunnett's test).

An inhibitor of importin-β significantly suppressed the PTEN nuclear translocation and directed migration following wounding (Figs. 3 and 4). The precise mechanism governing the nuclear translocation of PTEN remains unclear; however, it may be associated with the following mechanisms. PTEN nuclear accumulation is dependent on Ran-GTPase activity, suggesting the essential function of importin-β in this transport process (Gil *et al.* 2006). The importin-β family member Importin-11 (IPO11) transports PTEN into the nucleus and protects it from cytoplasmic proteins that cause PTEN degradation (Chen *et al.* 2017). In addition, cells can sense mechanical forces through a mechanosensitive complex and generate reactive oxygen species (ROS) (Chatterjee and Fisher 2014). Mechanical forces could induce the direct opening of hemichannels. Adenosine triphosphate (ATP) is released outside of the cell from hemichannels (Takada *et al.* 2014). The production of ROS and cellular ATP depletion results in increased nuclear PTEN (Du *et al.* 2017). Moreover, ubiquitination is known to control PTEN's nuclear localization (Baker 2007). Nedd4-1, an E3 ubiquitin-protein ligase, mediates PTEN monoubiquitination, regulating the nuclear import of PTEN (Trotman *et al.* 2007). In this study, after neighbor cell wounding, Importin-β and several other mechanisms could be associated with the entry of PTEN into the nucleus. Further studies are needed to determine whether importin-β directly interacts with NLS-like sequences and transports PTEN into the nucleus. Inhibition of PTEN nuclear localization inhibits directed migration after neighbor cell wounding, suggesting that, besides cell proliferation and cell stability, nuclear-localized PTEN may also be involved in directed cell migration in confluent cell monolayers.

PIP3 accumulated at the cell edge near the wounded cells (Fig. 5); Importazole suppressed the nuclear localization of

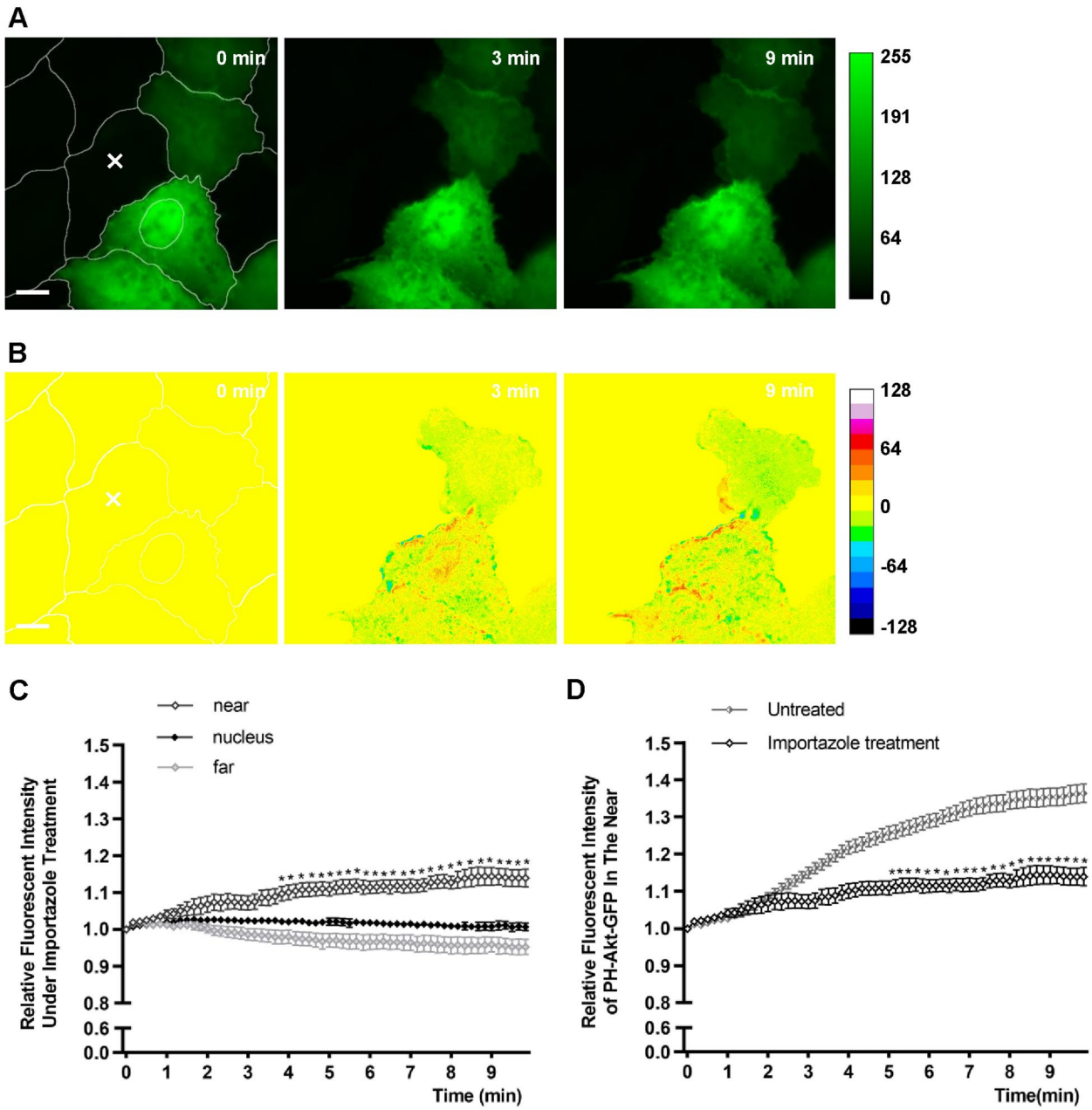

Figure 6. The dynamics of PH-Akt-GFP after neighbor cell wounding under Importazole treatment. (***A***) Representative fluorescence images of PH-Akt-GFP during treatment with Importazole (40 μmol L^{-1}) before directed migration. (***B***) Images of PH-Akt-GFP translocation obtained by subtracting the original image in (***A***) captured at $t=0$ min and setting the initial value as 0. The intensity of PH-Akt-GFP is shown using a pseudo color scale. Greater than 0 are considered an increase compared with the initial value. Cell boundaries and nucleus boundaries at 0 min are indicated by *white line*. "×" indicates the wounded cell. *White scale bar*: 10 μm. (***C***) Relative fluorescent intensity of PH-Akt-GFP under Importazole treatment. $N=8$, $n=14$. Mean ± standard error of the mean. $^{*}P<0.05$ vs. 0 min (two-way ANOVA with post hoc Dunnett's test). (***D***) Comparison of PH-Akt-GFP relative fluorescence intensity in the near ROI with Fig. 5*D*. $N=8$, $n=14$. Mean ± standard error of the mean. $^{*}P<0.05$ vs. untreated (two-way ANOVA with post hoc Sidak's test).

PTEN and the directional accumulation of PIP3 (Fig. 6). The mutually inhibitory relationship between PTEN and PIP3 regulates their localized levels, resulting in their spatial separation (Matsuoka and Ueda 2018). Additionally, PI3K signaling and PIP3 accumulation at the front edge of cells are important for promoting pseudopodia formation and directed cell migration (Chung *et al.* 2001; Blitsman *et al.* 2024). When importin-β is inhibited, cytoplasmic PTEN is not transported into the nucleus. Consequently, in the region near the wounded cells, undiminished cytoplasmic

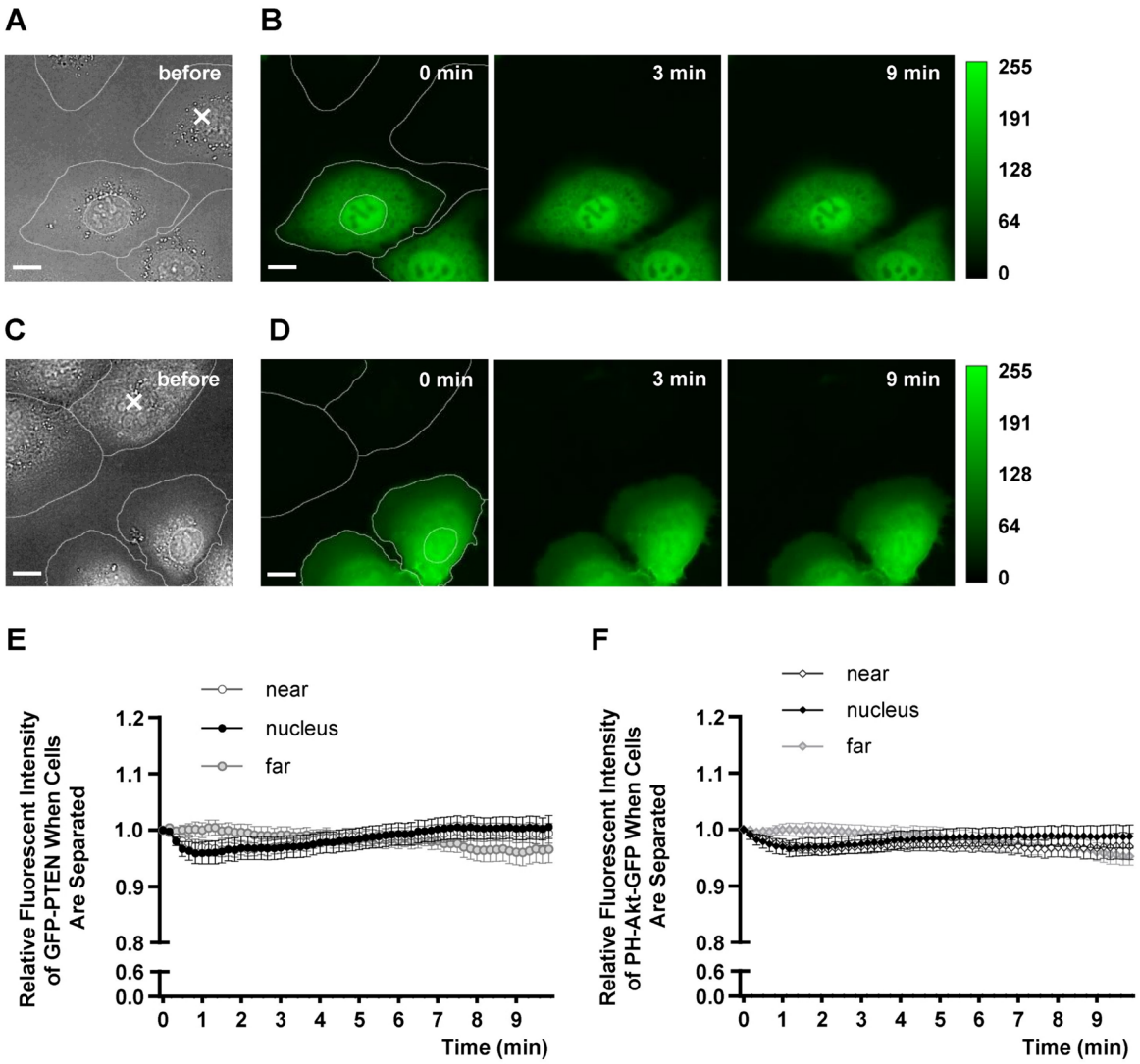

Figure 7. The dynamics of GFP-PTEN and PH-Akt-GFP after wounding when cells are separated. (***A***) Images of cells before wounding. (***B***) Representative fluorescence images of GFP-PTEN. (***C***) Images of cells before wounding. (***D***) Representative fluorescent images of PH-Akt-GFP. Cell boundaries and nucleus boundaries at 0 min are indicated by *white line*. "×" indicates the wounded cell. *White scale bar*: 10 µm. (***E***) Relative fluorescence intensity of GFP-PTEN in a time series. $N=6$, $n=9$. (***F***) Relative fluorescence intensity of PH-Akt-GFP in a time series. $N=6$, $n=10$. Mean ± standard error of the mean. $^{*}P<0.05$ vs. 0 min (two-way ANOVA with post hoc Dunnett's test).

PTEN converts PIP3 to PIP2, reducing PIP3 accumulation and thereby inhibiting cell elongation after wounding. These results suggest that the nuclear translocation of PTEN may regulate PIP3 accumulation by modulating cytoplasmic PTEN levels, thereby affecting cell migration in cell monolayers.

On the other hand, although the mechanisms of how signal transduction regulates PIP3 and PTEN are unclear, Protein kinase Cα (PKCα) and myristoylated alanine-rich C kinase substrate (MARCKS) may play a role. PKCα accumulates at the edges of the cells adjacent to wounded cells at an early stage (Sasaki *et al.* 2021). MARCKS, a major PKC substrate, binds to and modulates free PIP2 levels, which in turn, affects the recruitment of PI3K to the membrane (Ziemba *et al.* 2016). The displacement of MARCKS from the membrane results in increased PIP3 levels (Ziemba and Falke 2018). Therefore, after neighbor cell wounding, active PKCα accumulates at the edge near wounded cells, causing the dissociation of MARCKS from the membrane, and then, active PI3K phosphorylates PIP2 to form PIP3, which accumulates while PTEN decreases from the cell edge near wounded cells. The PKCα-MARCKS-PIP3 signaling transduction may play an important role in mediating the spatial distribution of PTEN.

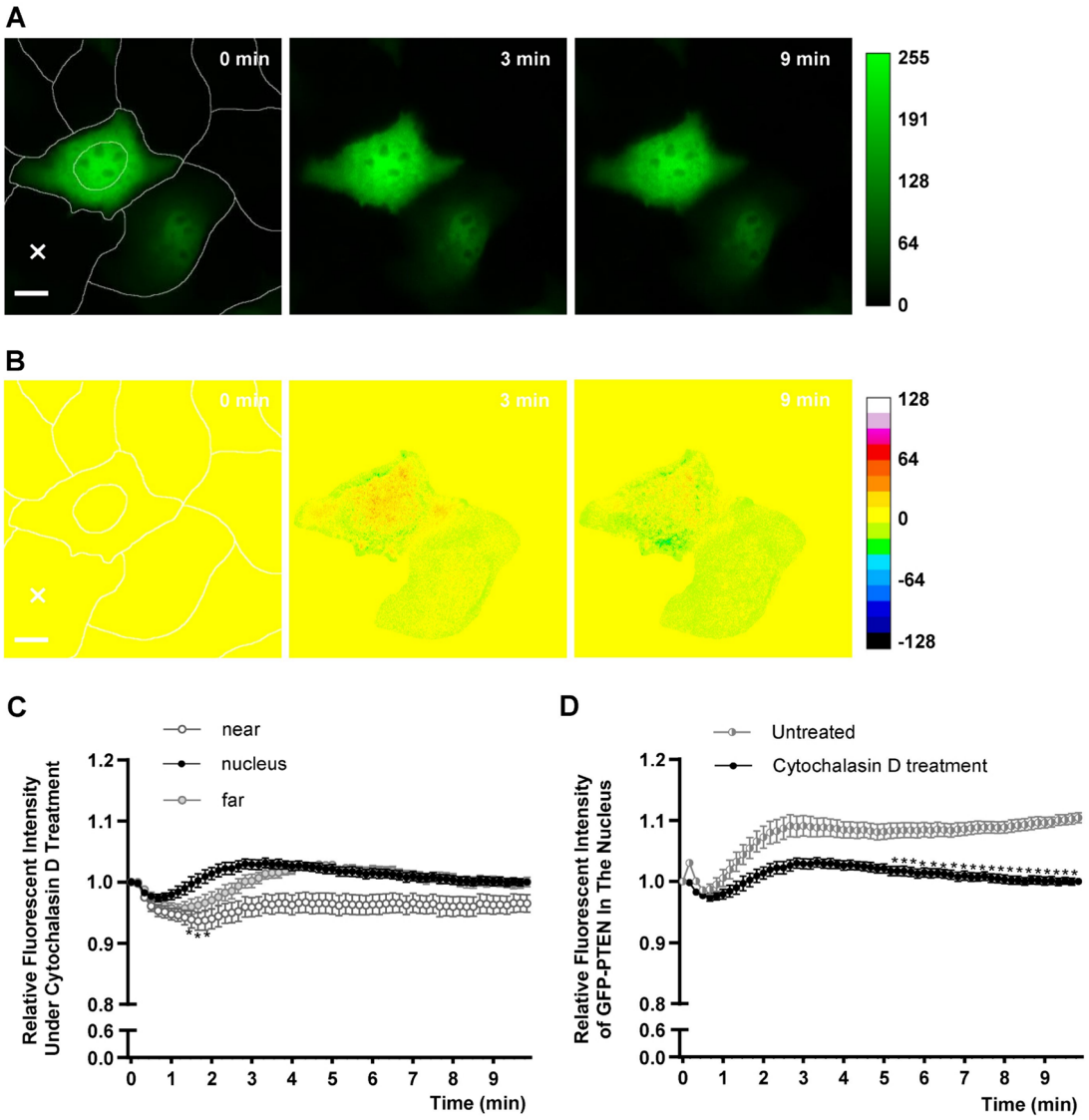

Figure 8. The effect of the actin inhibitor cytochalasin D. (***A***) Representative fluorescence images of GFP-PTEN under treatment with cytochalasin D (2.5 μmol L^{-1}) before directed migration. (***B***) Images of GFP-PTEN translocation obtained by subtracting the original image in (***A***) captured at $t=0$ min and setting the initial value as 0. The intensity of GFP-PTEN is shown using a pseudo color scale. Greater than 0 are considered an increase compared with the initial value. Cell boundaries and nucleus boundaries at 0 min are indicated by *white line*. "×" indicates the wounded cell. *White scale bar*: 10 μm. (***C***) Relative fluorescence intensity of GFP-PTEN in time series. $N=6$, $n=12$. Mean ± standard error of the mean. $^{*}P<0.05$ vs. 0 min (two-way ANOVA with post hoc Dunnett's test). (***D***) Comparison of GFP-PTEN relative fluorescence intensity in the nucleus with Fig. 2*E*. $N=6$, $n=12$. Mean ± standard error of the mean. $^{*}P<0.05$ vs. untreated (two-way ANOVA with post hoc Sidak's test).

Conclusions

Our study presents the first evidence of PTEN nuclear translocation before directed migration begins in cell monolayers, a process different from that in single cells. This translocation is critically dependent on cell–cell adhesion and mediated by importin-β and actin cytoskeleton signaling pathways, offering new insights into the regulatory mechanisms underlying directed migration in cell monolayers. Our findings highlight the pivotal role of PTEN translocation in mechanotransduction mechanisms within confluent monolayers. The intricate interplay between cell–cell adhesion, signal transduction, and PTEN's spatiotemporal distribution provides potential avenues for investigating tissue dynamics and cellular responses to wounding.

Supplementary Information The online version contains supplementary material available at https://doi.org/10.1007/s11626-024-00927-x.

Acknowledgements The authors would like to thank Enago (www.enago.jp) for the English language review.

Author contribution Quanzhi LU: investigation; data curation; formal analysis; writing—original draft; writing—review and editing. Saori Sasaki: investigation, data curation, validation. Toshihiro Sera: funding acquisition, supervision, methodology. Susumu Kudo: funding acquisition; writing—review and editing; supervision; conceptualization.

Funding This work was supported by JKA and its promotion fund from AUTORACE and JST SPRING program (grant number JPMJSP2136).

Data availability The data used and analyzed in this study are available from the corresponding author upon reasonable request.

Declarations

Ethics approval Not applicable.

Competing interests The authors declare no competing interests.

References

Arai M, Shimada T, Kora C *et al* (2017) Biphasic and directed translocation of protein kinase Cα inside cultured endothelial cells before migration. Biochem Biophys Rep 12:91–97. https://doi.org/10.1016/j.bbrep.2017.08.003

Arai Y, Shibata T, Matsuoka S *et al* (2010) Self-organization of the phosphatidylinositol lipids signaling system for random cell migration. Proc Natl Acad Sci USA 107:12399–12404. https://doi.org/10.1073/pnas.0908278107

Baker SJ (2007) PTEN enters the nuclear age. Cell 128:25–28. https://doi.org/10.1016/j.cell.2006.12.023

Blitsman Y, Hollander E, Benafsha C *et al* (2024) The potential of PIP3 in enhancing wound healing. IJMS 25:1780. https://doi.org/10.3390/ijms25031780

Campbell RB, Liu F, Ross AH (2003) Allosteric activation of PTEN phosphatase by phosphatidylinositol 4,5-bisphosphate. J Biol Chem 278:33617–33620. https://doi.org/10.1074/jbc.C300296200

Chatterjee S, Fisher AB (2014) Mechanotransduction in the endothelium: role of membrane proteins and reactive oxygen species in sensing, transduction, and transmission of the signal with altered blood flow. Antioxid Redox Signal 20:899–913. https://doi.org/10.1089/ars.2013.5624

Chen M, Nowak DG, Narula N *et al* (2017) The nuclear transport receptor Importin-11 is a tumor suppressor that maintains PTEN protein. J Cell Biol 216:641–656. https://doi.org/10.1083/jcb.201604025

Chung CY, Funamoto S, Firtel RA (2001) Signaling pathways controlling cell polarity and chemotaxis. Trends Biochem Sci 26:557–566. https://doi.org/10.1016/S0968-0004(01)01934-X

Chung J-H, Eng C (2005) Nuclear-cytoplasmic partitioning of phosphatase and tensin homologue deleted on chromosome 10 (PTEN) differentially regulates the cell cycle and apoptosis. Can Res 65:8096–8100. https://doi.org/10.1158/0008-5472.CAN-05-1888

Chung J-H, Ginn-Pease ME, Eng C (2005) Phosphatase and tensin homologue deleted on chromosome 10 (PTEN) has nuclear localization signal–like sequences for nuclear import mediated by major vault protein. Can Res 65:4108–4116. https://doi.org/10.1158/0008-5472.CAN-05-0124

Denning G, Jean-Joseph B, Prince C *et al* (2007) A short N-terminal sequence of PTEN controls cytoplasmic localization and is required for suppression of cell growth. Oncogene 26:3930–3940. https://doi.org/10.1038/sj.onc.1210175

Du Z, Dong C, Ren J (2017) A study of the dynamics of PTEN proteins in living cells using *in vivo* fluorescence correlation spectroscopy. Methods Appl Fluoresc 5:024008. https://doi.org/10.1088/2050-6120/aa6b07

Fife CM, McCarroll JA, Kavallaris M (2014) Movers and shakers: cell cytoskeleton in cancer metastasis: cytoskeleton and cancer metastasis. Br J Pharmacol 171:5507–5523. https://doi.org/10.1111/bph.12704

Friedl P, Alexander S (2011) Cancer invasion and the microenvironment: plasticity and reciprocity. Cell 147:992–1009. https://doi.org/10.1016/j.cell.2011.11.016

Funamoto S, Meili R, Lee S *et al* (2002) Spatial and temporal regulation of 3-phosphoinositides by PI 3-kinase and PTEN mediates chemotaxis. Cell 109:611–623. https://doi.org/10.1016/S0092-8674(02)00755-9

Gerisch G, Schroth-Diez B, Müller-Taubenberger A, Ecke M (2012) PIP3 waves and PTEN dynamics in the emergence of cell polarity. Biophys J 103:1170–1178. https://doi.org/10.1016/j.bpj.2012.08.004

Gil A, Andrés-Pons A, Fernández E *et al* (2006) Nuclear localization of PTEN by a Ran-dependent mechanism enhances apoptosis: involvement of an N-terminal nuclear localization domain and multiple nuclear exclusion motifs. MBoC 17:4002–4013. https://doi.org/10.1091/mbc.e06-05-0380

Gil A, Andrés-Pons A, Pulido R (2007) Nuclear PTEN: a tale of many tails. Cell Death Differ 14:395–399. https://doi.org/10.1038/sj.cdd.4402073

Gil A, Rodríguez-Escudero I, Stumpf M *et al* (2015) A functional dissection of PTEN N-terminus: implications in PTEN subcellular targeting and tumor suppressor activity. PLoS ONE 10:e0119287. https://doi.org/10.1371/journal.pone.0119287

Görlich D, Kutay U (1999) Transport between the cell nucleus and the cytoplasm. Annu Rev Cell Dev Biol 15:607–660. https://doi.org/10.1146/annurev.cellbio.15.1.607

Heering J, Erlmann P, Olayioye MA (2009) Simultaneous loss of the DLC1 and PTEN tumor suppressors enhances breast cancer cell migration. Exp Cell Res 315:2505–2514. https://doi.org/10.1016/j.yexcr.2009.05.022

Iijima M, Devreotes P (2002) Tumor suppressor PTEN mediates sensing of chemoattractant gradients. Cell 109:599–610. https://doi.org/10.1016/S0092-8674(02)00745-6

Jamora C, Fuchs E (2002) Intercellular adhesion, signalling and the cytoskeleton. Nat Cell Biol 4:E101–E108. https://doi.org/10.1038/ncb0402-e101

Li J, Tanhehco EJ, Russell B (2014) Actin dynamics is rapidly regulated by the PTEN and PIP_2 signaling pathways leading to myocyte hypertrophy. Am J Physiol Heart Circ Physiol 307:H1618–H1625. https://doi.org/10.1152/ajpheart.00393.2014

Lin JS, Shi Y, Peng H *et al* (2015) Loss of PTEN promotes podocyte cytoskeletal rearrangement, aggravating diabetic nephropathy: podocyte PTEN in diabetic nephropathy. J Pathol 236:30–40. https://doi.org/10.1002/path.4508

Liu F, Wagner S, Campbell RB *et al* (2005) PTEN enters the nucleus by diffusion. J Cell Biochem 96:221–234. https://doi.org/10.1002/jcb.20525

Matsuoka S, Ueda M (2018) Mutual inhibition between PTEN and PIP3 generates bistability for polarity in motile cells. Nat Commun 9:4481. https://doi.org/10.1038/s41467-018-06856-0

Mayor R, Etienne-Manneville S (2016) The front and rear of collective cell migration. Nat Rev Mol Cell Biol 17:97–109. https://doi.org/10.1038/nrm.2015.14

Mihai C, Bao S, Lai J-P *et al* (2012) PTEN inhibition improves wound healing in lung epithelia through changes in cellular mechanics that enhance migration. Am J Physiol Lung Cell

Mol Physiol 302:L287–L299. https://doi.org/10.1152/ajplung.00037.2011

Parent CA, Blacklock BJ, Froehlich WM *et al* (1998) G protein signaling events are activated at the leading edge of chemotactic cells. Cell 95:81–91. https://doi.org/10.1016/S0092-8674(00)81784-5

Peglion F, Capuana L, Perfettini I *et al* (2022) PTEN inhibits AMPK to control collective migration. Nat Commun 13:4528. https://doi.org/10.1038/s41467-022-31842-y

Planchon SM, Waite KA, Eng C (2008) The nuclear affairs of PTEN. J Cell Sci 121:249–253. https://doi.org/10.1242/jcs.022459

Raftopoulou M, Etienne-Manneville S, Self A *et al* (2004) Regulation of cell migration by the C2 domain of the tumor suppressor PTEN. Science 303:1179–1181. https://doi.org/10.1126/science.1092089

Ridley AJ, Schwartz MA, Burridge K *et al* (2003) Cell migration: integrating signals from front to back. Science 302:1704–1709. https://doi.org/10.1126/science.1092053

Saraswathibhatla A, Galles EE, Notbohm J (2020) Spatiotemporal force and motion in collective cell migration. Sci Data 7:197. https://doi.org/10.1038/s41597-020-0540-5

Sasaki S, Takahashi R, Luo Y *et al* (2021) Spatiotemporal distribution of PKCα, Cdc42, and Rac1 before directed cell migration. Biochem Biophys Res Commun 584:26–31. https://doi.org/10.1016/j.bbrc.2021.10.080

Scarpa E, Mayor R (2016) Collective cell migration in development. J Cell Biol 212:143–155. https://doi.org/10.1083/jcb.201508047

Schneider CA, Rasband WS, Eliceiri KW (2012) NIH Image to ImageJ: 25 years of image analysis. Nat Methods 9:671–675. https://doi.org/10.1038/nmeth.2089

Sera T, Arai M, Cui Z *et al* (2019) Unloading of intercellular tension induces the directional translocation of PKCα. Journal Cellular Physiology 234:9764–9777. https://doi.org/10.1002/jcp.27662

Servant G, Weiner OD, Herzmark P *et al* (2000) Polarization of chemoattractant receptor signaling during neutrophil chemotaxis. Science 287:1037–1040. https://doi.org/10.1126/science.287.5455.1037

Stambolic V, Suzuki A, de la Pompa JL *et al* (1998) Negative regulation of PKB/Akt-dependent cell survival by the tumor suppressor PTEN. Cell 95:29–39. https://doi.org/10.1016/S0092-8674(00)81780-8

Steck PA, Pershouse MA, Jasser SA *et al* (1997) Identification of a candidate tumour suppressor gene, MMAC1, at chromosome 10q23.3 that is mutated in multiple advanced cancers. Nat Genet 15:356–362. https://doi.org/10.1038/ng0497-356

Stock J, Pauli A (2021) Self-organized cell migration across scales – from single cell movement to tissue formation. Development 148:dev191767. https://doi.org/10.1242/dev.191767

Takada H, Furuya K, Sokabe M (2014) Mechanosensitive ATP release from hemichannels and Ca2+ influx through TRPC6 accelerate wound closure in keratinocytes. J Cell Sci. 147314. https://doi.org/10.1242/jcs.147314

Tamura M, Gu J, Matsumoto K *et al* (1998) Inhibition of cell migration, spreading, and focal adhesions by tumor suppressor PTEN. Science 280:1614–1617. https://doi.org/10.1126/science.280.5369.1614

Trotman LC, Wang X, Alimonti A *et al* (2007) Ubiquitination regulates PTEN nuclear import and tumor suppression. Cell 128:141–156. https://doi.org/10.1016/j.cell.2006.11.040

Vasioukhin V, Bauer C, Yin M, Fuchs E (2000) Directed actin polymerization is the driving force for epithelial cell–cell adhesion. Cell 100:209–219. https://doi.org/10.1016/S0092-8674(00)81559-7

Wakatsuki T (2001) Effects of cytochalasin D and latrunculin B on mechanical properties of cells. J Cell Sci 114. https://doi.org/10.1242/jcs.114.5.1025

Xu X, Meier-Schellersheim M, Jiao X *et al* (2005) Quantitative imaging of single live cells reveals spatiotemporal dynamics of multistep signaling events of chemoattractant gradient sensing in Dictyostelium. Molecular Biology of the Cell 16:676–688. https://doi.org/10.1091/mbc.e04-07-0544

Yamao M, Naoki H, Kunida K *et al* (2015) Distinct predictive performance of Rac1 and Cdc42 in cell migration. Sci Rep 5:17527. https://doi.org/10.1038/srep17527

Young P (2003) E-cadherin controls adherens junctions in the epidermis and the renewal of hair follicles. EMBO J 22:5723–5733. https://doi.org/10.1093/emboj/cdg560

Ziemba BP, Burke JE, Masson G *et al* (2016) Regulation of PI3K by PKC and MARCKS: single-molecule analysis of a reconstituted signaling pathway. Biophys J 110:1811–1825. https://doi.org/10.1016/j.bpj.2016.03.001

Ziemba BP, Falke JJ (2018) A PKC-MARCKS-PI3K regulatory module links Ca2+ and PIP3 signals at the leading edge of polarized macrophages. PLoS One 13:e0196678. https://doi.org/10.1371/journal.pone.0196678

Springer Nature or its licensor (e.g. a society or other partner) holds exclusive rights to this article under a publishing agreement with the author(s) or other rightsholder(s); author self-archiving of the accepted manuscript version of this article is solely governed by the terms of such publishing agreement and applicable law.